Preprint
UCRL-JC- 134961

# A Review of Astrophysics Experiments on Intense Lasers

*B.A. Remington, D. Arnett, R.P. Drake, H. Takabe*

This article was submitted to 41st Annual Meeting of the Division of Plasma Physics, Seattle, WA, November 15-19, 1999

**March 3, 1999**

U.S. Department of Energy
Lawrence Livermore National Laboratory

# A review of astrophysics experiments on intense lasers*

Bruce A. Remington
Lawrence Livermore National Laboratory, Livermore, CA, U.S.A.
remington2@llnl.gov

David Arnett
University of Arizona, Tucson, AZ, U.S.A.
dave@bohr.as.arizona.edu

R. Paul Drake
University of Michigan, Ann Arbor, MI, U.S.A.
rpdrake@umich.edu

Hideaki Takabe
Osaka University, Osaka, Japan
takabe@ile.osaka-u.ac.jp

UCRL-JC-131535
Resubmitted to Science on March 3, 1999

## ABSTRACT

Astrophysics traditionally has been the domain of large astronomical observatories and theorists' computers, the former producing images from deep space, and the latter constructing intricate models to explain the observations. A component often missing has been the ability to quantitatively test the theories and models in an experimental setting where the initial and final states are well characterized. In a new development, intense lasers are being used to recreate aspects of astrophysical phenomena in the laboratory, allowing the creation of experimental testbeds where theory and modeling can be quantitatively compared with data. We summarize here several areas of astrophysics: supernovae, supernova remnants, gamma-ray bursts, and giant planets. In each of these areas, experiments are under development at intense laser facilities to test and refine our understanding of these phenomena.

## INTRODUCTION

Modern intense lasers produce energy densities in sub-millimeter-scale volumes that are far larger than those produced in any other laboratory. This allows access in the laboratory to phenomena that otherwise appear only in energetic astrophysical systems. With these highly versatile laser facilities, matter can be prepared reproducibly in conditions that are equivalent, in a rigorously scaled sense, to those in large astrophysical systems such as supernovae, Herbig-Haro jets, or giant planets. Examples of areas that can be studied include strong shock phenomena; high Mach number jets; strongly coupled plasmas; compressible hydrodynamic instabilities; radiation flow; photoevaporation front hydrodynamics; and fundamental properties such as opacities and equations of state. Consequently, a vibrant new field of research is emerging – laboratory astrophysics with

intense lasers. This topic was the subject of a recent conference, the *2nd International Workshop on Laboratory Astrophysics with Intense Lasers,* held in Tucson, Arizona, March 19-21, 1998 (1)

Traditional laboratory astrophysics has generally focused on measuring fundamental parameters such as nuclear reaction cross sections and opacities. Nuclear fusion reactions are the fundamental energy source of the stars, and their cross sections quantify the individual reaction probabilities, allowing the heat production inside stars to be calculated. Opacities are the fundamental atomic properties that govern radiation transport within stars. Opacities quantify the probability that an atom will absorb photons that pass within its vicinity, and consequently control to a large extent the temperature profiles of the interiors of stars. These fundamental "input" quantities - cross sections and opacities - are required in models of phenomena such as stellar pulsations and supernova light curves. The new research emphasized here is aimed at probing astrophysical dynamics directly by creating scaled reproductions of the astrophysical systems in the laboratory. This allows the "output" of astrophysics theories and modeling to be tested directly, where the initial and final states are well characterized. Here we present a brief review of this emerging field, selecting out of the many possible topics supernovae, supernova remnants, gamma ray bursts, and high pressure equations of state (EOS) relevant to the giant planets for discussion.

## SUPERNOVAE

Core-collapse supernovae represent the dramatic endpoint of one of nature's most impressive cycles: the life and death of a massive star. (2, 3, 4, 5, 6) The final death throes of the star are spent in a high-stakes "tug of war" pitting quantum mechanical degeneracy pressure against the more familiar gravitational pressure. The outcome determines whether the final state is a white dwarf, neutron star, or black hole, and is based on the strength of the degeneracy pressure to withstand the radially inward tug of gravity. (7) Stars with initial masses of 1-8 $M_{sun}$ finish their hydrogen burning while their cores are not yet degenerate. They undergo core contraction, which raises the core density and temperature sufficiently to trigger He burning. These stars subsequently lose mass effectively, and end their lifetimes as white dwarfs, with masses of ~$0.6M_{sun}$. White dwarfs are supported by the pressure of the degenerate electrons in their interiors, that is, it is the quantum mechanical Pauli exclusion principle that prevents further collapse. The maximum mass possible for a white dwarf is the Chandrashekar limiting mass, $M_{Ch} \approx 1.4M_{sun}$. Larger stars have high enough temperatures in their cores to continue the nuclear fusion burning cycle up to Fe. Once the core reaches Fe, the nuclear fusion reactions no longer release net energy (because the nuclear binding energy per nucleon is maximum in Fe, at nearly 9 MeV/nucleon), and the thermonuclear fires are extinguished. The mass of the Fe core continues to grow as the surrounding layers burn their way to this thermonuclear endpoint until the Fe core mass exceeds ~$1.4M_{sun}$. At this point, there is no longer sufficient heat produced in the core to balance cooling by neutrino emission and photonuclear dissociation, and the core surrenders to gravity, triggering a catastrophic gravitational collapse that is over in a matter of seconds. This collapse is arrested only when the core density reaches that of degenerate nuclear matter (~$2 \times 10^{14}$ g/cm$^3$). The Fermi degeneracy pressure, $P_{deg} \sim \rho^{2/3}$, increases sufficiently to stop the implosion, and a spectacular nuclear rebound occurs whose strength is determined by the EOS of bulk nuclear matter. By a mechanism still debated, this launches the powerful outward-propagating shock that first "stalls" in the infalling matter, then gets re-energized by convection and by energy

deposition due neutrinos emitted from the core. The shock thus restarted, traverses the overlaying layers and effectively blows the star apart. Thus, the catastrophic end of the massive star marks the spectacular beginning of a core-collapse supernova. This explosive birth is observed as a bright flash of UV light, as illustrated by the calculated light curve for SN1987A in the inset of Fig. 1A (4, 8). If the core has a mass larger than 2-3$M_{sun}$, the core collapse continues to form a black hole.

**Supernova Light Curves**

The visual supernova (SN) commences when the shock breaks out through the surface of the star about an hour after the core collapses.(4) There is a sudden increase in temperature to 20-30 eV and luminosity, followed by a rapid drop in both quantities, as the star expands and cools adiabatically (Fig. 1A inset). About 30 minutes after shock breakout, the luminosity approaches a constant value, as the recombination front, which determines the photosphere, moves inward in mass at roughly the constant temperature (for hydrogen) of 6000 K. After some 20-40 days, the heat from the radioactive core, heated by Compton scattering of the $\gamma$-rays produced from $^{56}$Ni, $^{56}$Co, and $^{44}$Ti, reaches the photosphere, and the light curve rises up in a broad secondary maximum. (Fig. 1A) Subsequently, the decay of the light curve is monotonic in time at a rate determined by the half-lives of the various radioactive nuclei that serve as the heat source. The light curve contains a wealth of information about the star and its explosion. The luminosity varies directly with the explosion energy per unit mass, E/M, and is also proportional to the initial radius of the star. For the same E/M, SN from small stars are not as bright, since more energy goes into hydrodynamic expansion. The luminosity is on average inversely proportional to the opacity, since lower opacity means shorter radiative diffusion times. Finally, the light curve time evolution is sensitive to the degree that the core hydrodynamically mixes outwards into the envelope, bringing heat nearer to the photosphere. An ability to quantitatively calculate a SN light curve would allow the intrinsic brightness of the SN to be known. Comparison with the observed brightness would give its distance, through the expanding photosphere method (9, 10) Together with spectroscopic measurements of its redshift, this allows the Hubble constant, $H_0$, to be determined (11). There are several aspects to synthetic light curve calculations that could benefit from laboratory experiments, such as radiation flow, opacities, and hydrodynamic mixing.

Exploding stars create a homologous expansion, where each radiating region resides in a velocity gradient and sees plasma receding from it in all directions. For photons emitted in one region to escape the star, they have to pass through "windows" in opacity, where the absorption probability is low. In other words, the absorbing regions are always red shifted relative to the emitting regions. To be able to construct a synthetic light curve, requires that one calculate these "expansion opacities". Such calculations are very complex, and sophisticated opacity codes such as OPAL (12) are indispensable.

Experiments are being developed to test these difficult opacity calculations, focusing on atomic transitions that have not been explored previously. For example, in one experiment an iron foil 25 nm thick was sandwiched between two C layers and heated to ~20 eV using x-rays. The absorption spectrum near 730 eV was measured and analyzed, comparing several different opacity calculations (13) (Fig. 1B). Another experiment measured radiation line transport in an expanding plasma (14) (Fig. 1C). The experiment studied the structure of a doublet in the aluminum spectrum, at a wavelength near 7.18 Å. The emission occurs from an optically thick plasma with a significant velocity gradient, so

that emission in one line is often absorbed and re-emitted by the other line at another location in the plasma. The resulting line structure is complex, but can be reproduced by modeling only when this expansion effect on the radiation transport is taken into account. Hence, experiments are under development to test opacity calculations, both static and in expansion, relevant to SN light curves.

The 1D modeling of light curves such as those for SN1987A, even with the most sophisticated opacities, still fail to reproduce the time evolution. It appears that additional dynamics is at work. The modeling used to successfully reproduce the light curve for SN1987A shown in Fig. 1A assumes that the radioactive Ni, while centrally concentrated, was distributed half-way to the surface of the star. (4) This suggests that large scale hydrodynamic mixing had to have occurred after the $^{56}$Ni was synthesized in the core in the explosion. Hence, hydrodynamic instabilities appear to be an important ingredient in the dynamics of SN.

## Instabilities in the Explosion Phase

A core-collapse SN is driven by an extremely powerful shock, and strong shocks are the breeding ground of hydrodynamic instabilities. Two such instabilities seem particularly important: the Rayleigh-Taylor and Richtmyer-Meshkov instabilities. The Rayleigh-Taylor instability occurs when gravity tries to pull a heavier fluid through an underlying lighter one (for example, large air bubbles under water, or heated gas from a powerful explosion in the atmosphere). The Richtmyer-Meshkov instability is closely related, with the role of gravity replaced by the inertia from an impulsive acceleration due to a shock wave.

During the shock transit phase, the Richtmyer-Meshkov (RM) instability is triggered at each discontinuity in the density profile of the star, i.e., at the O-He and He-H "interfaces." After shock transit, hydrodynamic mixing continues due to the Rayleigh-Taylor (RT) instability, as the denser layers are decelerated by the lower density outer layers. The outward mixing of the higher-density, radioactive core material (eg., $^{56}$Ni, $^{56}$Co, $^{44}$Ti) brings the radioactive heat source towards the surface of the star. These explosion products decay by the emission of $\gamma$-rays, which Compton scatter off electrons in their vicinity. The consequent re-heating of the photosphere causes the secondary maximum in the light curve (Fig. 1A). The RT mixing induces this reinvigoration of the light curve to start earlier, broadening the secondary maximum. Observations of the light curve of SN1987A unambiguously showed this broadening of the secondary peak, suggesting enhanced transport from the core out to the photosphere. (2, 3) Two-dimensional calculations of the development of the mixing at the O-He and He-H interfaces using the supernova code PROMETHEUS (15, 16) show that spikes of denser oxygen, and helium penetrate outward into the less dense envelope of hydrogen, while bubbles of hydrogen move inward relative to the average location of the H/He boundary (Fig. 2A). This interpenetration occurs through the growth and nonlinear evolution of the Rayleigh-Taylor (RT) instability.

Laser-based experiments can generate strong-shock initiated nonlinear hydrodynamic mixing conditions similar to those found in SNe. In a set of experiments scaled to reproduce the hydrodynamics of the He-H interface of SN1987A about an hour after explosion, a strong shock was passed through an interface separating dense "core" material (Cu) from the lower density outer envelope ($CH_2$). (17, 18) A 2D sinusoidal ripple (1D wave vector) was imposed at the interface. The subsequent 2D growth due to the RM and RT instabilities was measured by x-ray backlighting. Spikes of Cu penetrating

upward into less-dense $CH_2$ were observed as a consequence of the Rayleigh-Taylor instability (Fig. 2B). This interpenetration was calculated in 2D with PROMETHEUS and the simulations reproduced the observations very well.

A theoretical look at the relation between the hydrodynamics occurring in the SN versus in the laboratory experiment shows that a rigorous mapping exists. Consider the He-H interface at 1600 sec in the SN and the Cu-CH interface at 20 ns in the laser experiment. In both settings, the Reynold's number (the ratio of the inertial to the viscous force) and the Peclet number (the ratio of the convective to the conductive heat transport) are large. Therefore, viscosity and thermal diffusivity are negligible, and the dynamics of the interface are well described by Euler's equations for a polytropic gas (19),

$$\rho\left(\frac{\partial \mathbf{v}}{\partial t}+\mathbf{v}\cdot\nabla\mathbf{v}\right)=-\nabla p \ ,$$

$$\frac{\partial \rho}{\partial t}+\nabla\cdot(\rho\mathbf{v})=0 \quad , \quad \text{and}$$

$$\frac{\partial p}{\partial t}-\gamma\frac{p}{\rho}\frac{\partial \rho}{\partial t}+\mathbf{v}\cdot\nabla p-\gamma\frac{p}{\rho}\mathbf{v}\cdot\nabla\rho=0 \quad , \qquad (1)$$

which represent conservation of momentum, mass, and entropy, respectively. It is straight forward to show by substitution that Eq. 1 is invarient under the following scale transformation,

$$\begin{aligned} h_{SN} &\rightarrow a h_{lab}, \\ \rho_{SN} &\rightarrow b\rho_{lab}, \\ p_{SN} &\rightarrow c p_{lab}, \\ \tau_{SN} &\rightarrow a(b/c)^{1/2}\tau_{lab}, \end{aligned} \qquad (2)$$

where h, $\rho$, p, and $\tau$ correspond to characteristic spatial, density, pressure, and time scales, and subscripts *SN* and *lab* refer to the supernova and laboratory laser experiment, respectively. When transformation (2) is inserted into Eq. (1), the constants a, b, and c cancel, and the dynamics described by Euler's equation are indistinguishable in the SN and the laser experiment. Both settings are probing the same physics. Any insights gained through the laser experiment apply directly to the SN through the mapping described by Eq. 2. For example, the hydrodynamics illustrated in Figs. 2a and 2b are similar, and can be related through the SN-to-laboratory mapping of h, $\rho$, p, $\tau$, and $g=\nabla p/\rho$ (Eq. 2) giving $10^{11}$ cm to 50 $\mu$m, $8\times10^{-3}$ g/cm$^3$ to 4 g/cm$^3$, 40 Mbar to 0.6 Mbar, and $10g_o$ to $10^{10}$ $g_o$, where these values were taken at times of 2000 sec for the SN and 20 ns for the laboratory experiment. (19)

An example where laboratory experiments can generate valuable insights relative to the star is the comparison of RT instability growth in 2D versus 3D. PROMETHEUS simulations comparing the evolution of RT bubbles and spikes in two and three dimensions in a proposed laboratory experiment show that single-mode 3D perturbations should penetrate 30-50% farther than those in 2D, an effect which may contribute to the early rise in the secondary maximum at day ~30 in the light curve of SN1987A. (2, 3) Initial laboratory results confirm this difference for single-mode perturbations. (20)

## SUPERNOVA REMNANTS

While SN explosions mark the end of a massive star, they also mark the beginning of its new life as a supernova remnant (SNR). Well known examples of SNRs such as the remnants of Tycho's SN (21), Keplers SN (22), the Cygnus loop (23), SN1006 (24), and the Crab nebula (25) provide exquisite visual testimony to their violent births. There are several active areas of research regarding the dynamics and evolution of SNRs which may be better understood with laser experiments.

### Shocks in the Supernova Remnant Phase

Shock dynamics dominate the evolution of supernova remnants (SNRs). The rapidly expanding ejecta from the supernova drive a shock forward into the surrounding medium, and a reverse shock forms where the ejecta are decelerated by the accumulating, shocked matter. The place where the ejecta and ambient medium meet, called the contact discontinuity, becomes hydrodynamically unstable. Currently the most actively observed SNR is the young remnant forming around SN1987A. This remnant consists of the standard SN ejecta expanding into the ambient medium, as well as a mysterious inner and two outer circumstellar nebular rings, which apparently existed prior to the SN explosion. Various models have been proposed for these rings, but as of yet no explanation fully explains their origin. The SN ejecta, however, are moving very fast (~$10^4$ km/s) compared to the nearly static (~10 km/s) inner ring, which has a diameter of ~1 light year. It is widely expected that the ejecta-forward shock system will impact the inner edge of the inner ring within the next ~5 years. This should launch a strong shock into the ring, heating it to 100-300 eV temperatures, and cause emissions at all wavelengths, from optical to x-ray. Careful observation of this impact should shed light on the structure, composition, and hopefully origin of the rings. Recent images of the inner ring (26, 27, 28) show a rapidly brightening, localized hot spot (upper right corner of Fig. 3A), suggesting that perhaps the collision of the forward shock with the ring has actually started. Spectral imaging of Lyman-$\alpha$ radiation, which is produced at the reverse shock, indicate that the reverse shock has traversed about 70% of the distance from the ring to the star. (26)

Laser experiments can produce shock structures similar to those in a SNR, under well-scaled hydrodynamic conditions. (19, 29, 30, 31) Experiments have been developed in 1D to reproduce the basic dynamics of SNR formation: fast-moving shock-induced ejecta sweeping into a surrounding low density, static ambient atmosphere. This launches a forward shock into the ambient medium and a reverse shock into the stagnating ejecta (Fig. 3B), much like the dynamics of SNR formation. Indeed, the laboratory experiment can be modeled by the self-similar model of Chevalier (32) developed to describe the 1D dynamics of SNRs.

Expectations are that the contact discontinuity (the meeting point of the ejecta and ambient plasmas) will be hydrodynamically unstable, and 2D experiments have commenced to look at this. One of the driving motivations for studying SNR physics relevant to SN1987A is the long-awaited impact of the SN blast wave with the inner circumstellar nebular ring. The interaction of the shock with the ring is sure to be rich in 3D, strong shock effects. A laser experiment is being developed to elucidate the 3D nature of the interaction of a strong shock with a localized high density feature such as a sphere. (33) The 3D development strongly affects the interactions, with azimuthal (3D) modes growing, and enhancing the "shredding" of the sphere. A similar 3D effect is likely for the

interaction of the SN1987A blast wave with the inner ring, and in shock-cloud interactions in general. (34)

Under the current conditions for the remnant of SN1987A, the scale transformation based on Euler's Equations described above for the explosion hydrodynamics might be applied again. For this to be relevant, one has to consider whether the shock is radiative, and whether the ambient magnetic field localizes the plasma. For the current conditions of SN1987A, the plasma density is low enough that the shocks are not radiative, that is, the radiative cooling time scale is long compared to a hydrodynamic time scale, $\tau_{rad}/\tau_{hydro} >> 1$. Also, the ambient magnetic field, B = ~100 μGauss, is large enough that the ion Larmor radius is much smaller than spatial scales of interest. Hence, the plasma can be treated hydrodynamically, the dynamics can be treated again with Euler's equations, Eq. 1, and the same rigorous scale transformation (Eq. 2) holds. For the SNR-to-laboratory transformation corresponding to the 1D experiment shown in Fig. 3B, we get 0.03 light year mapping to 100 μm, $10^4$ km/s to 60 km/s, and 1 year mapping to 1 ns (19), where these values correspond to times of 13 years in the SNR and 8 ns in the laboratory experiment.

Another well known remnant, SN1006 (Fig. 4A), is a good example of how shock wave analysis techniques applied to recent images provide insights into the supernova that exploded in the year 1006 at a distance of 2 kpc. (24) Spectral analysis of shock induced astrophysical emissions can yield the temperature, density, degree of equilibration, ionization state, and velocity of the shock. With an additional measure of the proper motion of the shock, the distance to the emitting source can also be determined. Such analysis of the shock-induced emissions from the remnant of SN1006 is given in Fig. 4B. Here, emission lines from hydrogen (Lyman β) and from 5-times-ionized oxygen (O VI) are identified. This is an example of emissions from a "non-radiative" shock – a shock traversing a low-enough density medium that the plasma behind the shock front is not cooling rapidly by radiation, $\tau_{rad}/\tau_{hydro} >> 1$. The conclusion from this spectral analysis is that plasma turbulence in the shock front is not effective in producing temperature equilibration among the different ion species.

A long-standing mystery regarding astrophysical shocks is whether or not the electrons are strongly heated by the magnetized turbulence at the shock fronts of SNRs (35). The impact of electrons upon emitting ions dominates the production of some emission lines, while the impact of protons dominates other emission lines. In the case of the shocks of the remnant from SN1006 and in several other cases analyzed to date, the electron temperature is found to be considerably below the ion temperature, $T_e \approx T_i/4$, for a Mach-50 shock (24). This provides evidence that the magnetized turbulence at the shock wave does not rapidly force equilibration of the electrons and the ions. Developing an experimental setting to check the theories and analysis techniques of astrophysical shocks seems possible, at least for some situations, and would be very beneficial.

Laser-based experiments can produce strong shock waves for study in a variety of ways. In an experiment using a table-top laser, a gas jet target produces an assembly of clusters of atoms of order 10 nm in size, each containing thousands of atoms. These clusters absorb the laser radiation from a 800 nm Ti:Sapphire laser with a pulse duration of 0.1 ps or less. This produces intense heating, disassembly of the clusters ("Coulomb explosion"), and radial expansion of the 2 mm long by initially 50 μm diameter laser-irradiated hot, cylindrical channel (36, 37, 38). Under sufficiently collisional conditions (Fig. 4C), a Mach ~40 shock wave forms that drives the surrounding gas outward. (39) Whether a magnetized shock can also be produced by this technique remains a topic for ongoing research, but an initial assessment looks promising (40). Given the high initial

temperature of the shock, and the ability to experimentally vary the density and gas species, creating radiative and non-radiative shocks should be possible by this technique.

In astrophysical systems and the laboratory, shocks can be produced for which radiation is essential to the dynamics. Radiation from the shock wave can cause preheat, altering the conditions ahead of the shock wave, and the shock-generated radiation can be an important component of the energy flow within the system. An example from astrophysics is SN 1993J, whose progenitor was a red supergiant star, surrounded by a very dense stellar wind. [41] The resulting shock structure was strongly radiative and this affected the subsequent shock dynamics, leading to significantly higher densities behind the shock front. Laboratory shocks in which radiation affects the dynamics can also be created and studied. An experiment in which low-density foam was directly illuminated with an intense laser has been carried out [42], generating shocks whose radiation affected the matter ahead of them. Another radiative shock experiment (43, 44) has been conducted where the shock was launched by irradiating a foam target with soft x-rays rather than direct laser illumination. Here, in three separate experiments conditions were created corresponding to (1) pure hydrodynamics (subsonic radiation wave), (2) pure radiation flow (supersonic radiative wave), and (3) intermediate dynamics ("transonic" regime). For each case, spectroscopy was used to determine the temperature profile in the plasma. For the case of the subsonic radiation front, the temperature behind the shock was determined spectroscopically, as shown in Fig. 4D. What remains is to develop the theoretical transformation, mapping the conditions of astrophysical radiative shocks such as those associated with the remnant of SN1993J (41) to the laboratory, so that these laser experiments can be turned into properly scaled reproductions of their astrophysical counterparts.

## GAMMA RAY BURSTS

Gamma-ray bursts (GRB) are the greatest enigma in contempory astrophysics (45, 46, 47, 48, 49). Detected at a rate of more than one per day from random directions in the sky, GRBs typically have burst durations of a few seconds, at photon energies of 0.1-10 MeV (Fig. 5A, 5B). GRB distances remained unknown for the past two decades, primarily because their radiation in all other wavelengths other than $\gamma$-rays was undetected. This changed recently with the determination of accurate positions (to within about 3 minutes of arc), obtained within hours of outburst by the BeppoSAX satellite. Optical spectoscopy of the light associated with the outburst, the ``afterglow", established that at least some of the GRBs are at cosmological distances of several billion light years (redshifts of $\Delta\lambda/\lambda = 1$ to 3). To generate the observed luminosities then requires total source energies of $\sim 10^{53}$ ergs/burst. The rapid rise time and rapid variability, $\Delta t \sim 1$ ms, observed in some bursts (Fig. 5A) imply a source size, $R_i \sim c\Delta t \sim 10^7$ cm, ie, these tremendous total energies appear to be emitted from very compact sources. The observed photon energy spectra can extend to ~100 MeV, have a power-law shape (Fig. 5B), and are well fit with a simple functional form,

$$N(E)dE \sim E^{-\alpha}dE ,$$

with spectral index $\alpha \sim 2$. This suggests that the source plasma is optically thin to the radiation observed. (If the source plasma were optically thick, the photons would thermalize, and the observed spectrum would have a Planckian, not a power-law shape.) This presents a problem. When two photons with energies $E_1$ and $E_2$ interact, their center-

of-mass energy is $\sim 2(E_1E_2)^{1/2}$, and the interaction can produce an $e^+e^-$ pair if $(E_1E_2)^{1/2} > m_ec^2$. (45) Denote the fraction of photon pairs in a GRB satisfying this condition as $f_p$. The optical depth (OD) for the $\gamma\gamma \rightarrow e^+e^-$ process, varies as $OD \sim f_p/R_i^2$, and is very large. Pairs are produced prodigiously, and by Compton scattering, they would make the plasma optically thick, thermalizing the photon spectrum. The observed spectra, however, are nonthermal, hence the "compactness problem". The fireball model was developed to resolve this problem without introducing "new physics". In this model, the source creates a relativistically expanding fireball so that the emission region is moving towards the observer at relativistic velocities. (45, 49) Consider a source of radiation moving towards an observer at rest with a relativistic velocity characterized by a Lorentz factor, $\Gamma = 1/(1-v^2/c^2)^{1/2} >> 1$. The observer detects photons with energy $h\nu_{obs}$, whereas these photons in the rest frame of the emission region, have energy $h\nu_{obs}/\Gamma$. Hence, at the emitter, the fraction of photons with energies high enough to produce $e^+e^-$ pairs, $f_p$, is reduced by a factor $\Gamma^{-2\alpha}$. Also, the emitting region appears Lorentz contracted, so that in its rest frame, the emission region is larger, with $R_i \sim \Gamma^2 c\Delta t$. The result is that the optical depth for the process $\gamma\gamma \rightarrow e^+e^-$ now varies as $OD \sim f_p/\Gamma^{4+2\alpha}R_i^2$, which for $\Gamma > \sim 100$ resolves the compactness problem. Through the blue shift boost, we observe the high energy photons, but the emission region remains optically thin, giving the observed $\gamma$-ray power-law spectrum. The kinetic energy of the GRB ejecta is assumed to be randomized behind internal ("reverse") shocks, and emitted as high energy photons when the shock is at a radius of $r_{int} = \Gamma^2 c\Delta t = 10^{12}$-$10^{13}$ cm, for $\Gamma = 100$-$300$. The "afterglow" is assumed to happen from emissions behind the external ("forward") shock at a radius of $r_{ext} > \sim 10^{17}$ cm.

Most GRBs show variability on time scales much shorter than (typically one hundredth of) the total GRB duration. (48) In the fireball model, such variability comes from internal ("reverse") shocks, which convert a substantial part of the directed kinetic energy to internal energy. This energy is then radiated as $\gamma$-rays by synchrotron and inverse-Compton emission of shock-accelerated electrons. The GRB overall duration reflects the duration over which energy is emitted from the source. Following internal shocks, the fireball rapidly cools and continues to expand, driving a relativistic blastwave into the surrounding interstellar medium gas. This external shock continuously heats new gas, and produces relativistic electrons that may produce the delayed radiation observed on time scales of days to months, that is , the afterglow. So, a relativistically expanding fireball produces the rapidly varying, hard x-rays by internal shocks, and the longer lived slow "afterglow" decay by the external shock.

Despite its qualitative successes, the fireball model is incomplete. The cause of GRBs is unknown, but must be spectacular because such great distances require enormous energies for the burst to appear so bright. The merger of a binary pair of neutron stars, the core collapse of a failed supernova, and other exotic events involving black holes and relativistic jets have been suggested. (45, 46) Radiation escapes the fireball only after it expands to radii many orders of magnitude larger than the original size of $\sim 10^7$ cm. The $\gamma$-ray emission occurs when the source has expanded to $\sim 10^{13}$ cm and the afterglow at $>10^{16}$ cm. Hence, the observed radiation does not provide direct information on the underlying source. The predictions of gamma-ray emission from the fireball involve the interaction of plasma with shocks moving at relativistic velocities and with magnetic fields. The details of this interaction are not understood. This superheated conglomerate is thought to expand relativistically in a fiery ball or jet of plasma, with copious production of $e^+e^-$ pairs. Explosion energies are estimated to be in the range of $10^{52}$ -$10^{53}$ erg (approaching the rest mass energy of the Sun!). Figure 5C shows results of Monte Carlo simulations of the $\gamma$-

ray spectrum of a GRB (50), using a model in which energetic electrons and positrons from the fireball produce $\gamma$ rays through multiple Compton upscattering of low-energy photons. This model qualitatively reproduces the observed GRB spectra and time evolution. A related phenomenon is the origin of ultra-high energy cosmic rays ($10^{20}$ eV), which are thought to occur by the Fermi acceleration mechanism at the fireball wave front (47).

Aspects of the underlying fireball physics may be accessible in the lab. In experiments under development to benchmark astrophysical codes for radiation hydrodynamics, a radiative, high Mach number jet has been created and characterized. (51) Here, the initial conditions were a hot (~1 keV), high velocity (~700 km/s), jet of highly ionized Au plasma, where the radiative cooling effects were large. Perhaps more relevant are experiments under way using the ultra-high intensity laser called the Petawatt. (52) Here, planar targets are irradiated by a laser pulse ($10^{20}$ W/cm$^2$), producing an expanding high energy-density wave of hot plasma, that is, a "laboratory fireball". The initial plasma temperature is thought to be several MeV, the plasma is relativistically hot, and electron-positron pairs are created. For the highest intensity shots, electrons have been observed up to energies of 100 MeV, and positron energy spectra have also been recorded (Fig. 5D). (53) Perhaps most interesting in these experiments is the excitation of nuclear states in the ~20 MeV range. The energetic electrons yield high energy x-rays through bremsstrahlung (Fig. 5E), which excite the nucleus through the giant dipole resonance. The nucleus de-excites by $\gamma$-ray emission or by emitting a nucleon. Photoneutron interactions can leave the nucleus in long-lived excited states that can be counted after the fact by $\gamma$-ray spectroscopy. The exact laser-plasma dynamics and subsequent plasma fireball evolution are still being worked out. But what is clear is that plasmas have now been created in the laboratory with a T ~ 1 MeV "thermal" component, and a higher energy tail. (52, 53) Significant $e^+e^-$ production, and excited nuclear levels have been observed. Hence, aspects of the underlying gamma-ray burst fireball physics, such as relativistic plasma effects, are becoming accessible in the laboratory.

## GIANT PLANETS

The "high stakes tug of war" between quantum mechanical degeneracy pressure and the more familiar gravitational pressure was discussed above in the section on supernovae. A somewhat more benign envirnoment to consider strong degeneracy effects is in the steady state interiors of the giant planets such as Saturn and Jupiter and the newly discovered brown dwarfs, (7, 54, 55, 56) as represented by the phase diagram shown in Fig. 6a (57). Here, because of their lower mass, $M \leq 0.08M_{sun}$, these bodies never ignite as stars, and the degeneracy pressure and strongly coupled effects dominate.

Strongly coupled plasmas are typically characterized by the dimensionless parameter, $\Gamma=(Ze)^2/akT$, where $a$ is a characteristic separation distance between ions. In plasmas with $\Gamma<<1$, thermal effects dominate and the plasma is considered "ideal". When $\Gamma \geq 1$, the Coulomb interactions become an equal player, and the plasma enters the strongly coupled regime, represented by the region to the right and below the $\Gamma=1$ line in Fig. 6a. When $\Gamma > 178$, the plasma becomes so strongly coupled that the ions freeze solid into a crystal lattice. Also, when the densities are high enough or temperatures low enough that $kT < \varepsilon_F$, where $\varepsilon_F = p_F^2/2m_e = (1/8)(3/\pi)^{2/3}(h^2/m_e)n_i^{2/3} \propto \rho^{2/3}$ is the Fermi energy, the plasma is called degenerate, and is represented by the region to the right and below the $\varepsilon_F = kT$ line in Fig. 6a. Here, electron degeneracy pressure becomes a major part of the total pressure. The isentropes for Jupiter and the brown giant G1229B (56) shown in Fig. 6a

indicate that these bodies, which are made up predominantly of H and He, are both strongly coupled and highly degenerate. Hence, the internal structure, $\rho(r)$, $T(r)$, and to some extent the external magnetic fields of the giant planets are determined by the equation of state (EOS) of degenerate hydrogen and helium at high pressure, P = 1-100 Mbar. The EOS of strongly-coupled, degenerate plasma, however, is notoriously difficult to calculate from first-principles theories, due to the complexity of including quantum mechanical effects into classical thermodynamic theories. Experiments in this parameter regime are a vital component in efforts to improve our understanding of Jupiter, the other giant planets, and brown dwarfs.

The EOS of a material can be determined by measuring its response to a known applied pressure. Measurements of the EOS of cryogenic deuterium, D, (an isotope of hydrogen) at applied pressures ranging from 220 kbar to 3.4 Mbar have been made on the Nova laser (57). In these experiments, the transition of hydrogen from a molecular fluid insulator phase to a monatomic metallic phase was unambiguously observed. A clear departure from the standard theoretical EOS models for hydrogen was found in the compressibility of $D_2$ in this regime (Fig. 6B). The results were consistent with a new model that included the potential energy sink caused by molecular dissociation ($D_2 \rightarrow$ D+D). These results, together with extensive results form gas-gun experiments at lower pressure (58, 59), have implications for the composition and dynamics of the outer layers of Jupiter, the other giant planets, and brown dwarfs.

The pressure and temperature in the mantle of Jupiter near the surface are in the range of 1-3 Mbar and a fraction of an eV. Deeper in the interior, the pressure and temperature increase, rising to 40 Mbar and a couple of eV at the center. (58) Near the surface, hydrogen exists as the molecule $H_2$, but dissociates to H+H and ionizes deeper in the mantel. This transition of hydrogen from insulator to conductor is important, because conducting H in the convective zone is thought create the 10-15 Gauss magnetic field of Jupiter. One of the fundamental open questions about the interior of Jupiter is whether there is a sharp boundary, a plasma phase transition (PPT), between a molecular hydrogen mantle and a monatomic hydrogen core at a radius of ~0.75 $R_J$ and pressure of 3 Mbar. The regimes accessed by the laser and gas-gun experiments represented on Fig. 6B span this critical transition from mantle to core of Jupiter, and suggest that a sharp discontinuity between molecular (mantle of Jupiter) to monatomic (core of Jupiter) hydrogen does not exist. The experiments (57, 60, 61) suggest that on the Jovian isentrope molecular hydrogen probably begins to dissociate at 400 kbar and dissociation continues smoothly to completion at ~3 Mbar, with metallization occurring right in the middle of this region at ~1.4 Mbar and ~4000 K. It now seems likely (60) that currents near the surface of Jupiter, at radii out to $0.95R_J$ contribute to the surface magnetic field, whereas previously it was thought that the magnetic field was formed deeper in the interior at ~0.75 $R_J$. The EOS of astrophysically relevant materials are being measured on other lasers as well, including LULI (62), Vulcan (62, 63), Helen (60, 64), Astrix (65), Gekko (66), and Shenguang-I (67). This whole area of measuring high pressure EOS on intense lasers represents fertile new territory for planetary and astrophysics research.

*The work was carried out under the auspices of the U.S. Department of Energy by the Lawrence Livermore National Laboratory under contract number W-7405-ENG-48.

## REFERENCES


1. http://lasers.llnl.gov/lasers/target/astro
2. W. D. Arnett, J. N. Bahcall, R. P. Kershner, S. E. Woolsey, Ann. Rev. Astron. Astrophys. **27**, 629-700 (1989).
3. W. Hillebrandt, P. Höflich, Rep. Prog. Phys. **52**, 1421 (1989).
4. David Arnett, *Supernovae and Nucleosynthesis* (Princeton Univ. Press, 1996).
5. H. Bethe Rev. Mod. Phys. **62**, 801 (1990).
6. Stan Woosley and Tom Weaver, Scientific American, 32 (Aug. 1989).
7. H.M. Van Horn, Science **252**, 384 (1991).
8. D. Arnett , submitted, Ap. J. Suppl. (Jan. 1999).
9. B.P. Schmidt *et al.*, Ap. J. **395**, 366 (1992); *ibid*, **432**, 42 (1994).
10. R.G. Eastman *et al.*, Ap. J. **466**, 911 (1996); ibid, **430**, 300 (1994).
11. D. Branch *et al.*, Phys. Plasmas **4**, 2016 (1997).
12. C. A. Iglesias, F. J. Rogers, Ap. J. **464**, 943-53 (1996).
13. C. Chenais-Popovics, submitted to Ap. J. Suppl. (Jan. 1999).
14. J. Wark *et al.*, Phys. Plasmas **4**, 2004 (1997); Phys. Rev. Lett. **75**, 1680 (1994); P.K. Patel *et al.*, submitted, JQSRT (1999).
15. E. Muller, B. Fryxell, D. Arnett, A&A **251**, 505-514 (1991).
16. B. Fryxell, E. Muller, D. Arnett, Ap. J. **367**, 619-34 (1991).
17. J. Kane *et al.*, Ap. J. **478**, L75-L78 (1997).
18. B. A. Remington *et al.*, Phys. Plasmas **4**, 1994-2003 (1997).
19. D.D. Ryutov *et al.*, ApJ , in press (June, 1999).
20. M.M. Marinak *et al.*, Phys. Rev. Lett. **75**, 3677 (1995).
21. U. Hwang, J.P. Hughes, and R. Petre, Ap. J. **497**, 833 (1998); P.F. Velazquez *et al.*, A&A **344**, 1060 (1998).
22. K.J. Borkowski and A.E. Szymkowiak, Ap. J. 477, L49 (1997); R. Braun, A&A **171**, 233 (1987); E. Dwek, Ap. J. **322**, 812 (1987).
23. N.A. Levenson *et al.*, Ap. J. Suppl. **118**, 541 (1998); Ap. J. **484**, 304 (1997); *ibid*, 468, 323 (1996); J.J. Hester *et al.*, Ap. J. **420**, 721 (1994); R.A. Resen *et al.*, A.J. **104**, 719 (1992).
24. J. C. Raymond, W. P. Blair, K. S. Long, Ap. J. **454**, L31-L34 (1995); P.F. Winkler and K.S. Long, Ap.J. **486**, L137 (1997); *ibid* **491**, 829 (1997).
25. J. Hester *et al.*, Ap. J. **456**, 225 (1996).
26. E. Michael, R. McCray, K. J. Borkowski, C. S. J. Pun, G. Sonneborn, in preparation (1999).
27. K. J. Borkowski, J. M. Blondin, R. McCray, Ap. J. **477**, 281-93 (1997).
28. K. J. Borkowski, J. M. Blondin, R. McCray, Ap. J. **476**, L31-L34 (1997).
29. R. P. Drake *et al.*, Ap. J. Lett. **500**, L157-L161 (1998).
30. R. P. Drake *et al.*, Phys. Rev. Lett. **81**, 2068 (1998).
31. J. Kane, R. P. Drake, B. A. Remington, Ap. J. **511**, 335 (1999).
32. R.A. Chevalier, Ap. J. **258**, 790 (1982).
33. R.I. Klein *et al.*, submitted, Ap. J. Suppl. (Jan. 1999); and in preparation (1999).
34. R. Klein *et al.*, Ap. J. **420**, 213 (1994).
35. J. M. Laming, J. C. Raymond, B. M. McLaughlin, W. P. Blair, Ap. J. **472**, 267-74 (1996).
36. T. Ditmire *et al.*, Phys. Rev. Lett. **78**, 2732-5 (1997); *ibid*, **78**, 3121-4 (1997); Nature **386**, 54-6 (1997); submitted, Ap. J. Suppl. (Jan. 1999).
37. G.S. Sarkisov *et al.*, JETP Letters **66**, 828 (1997).

38. S.Y. Chen *et al.*, Phys. Rev. Lett. **80**, 2610 (1998).
39. K. Shigemori, T.R. Ditmore, T. Kuhl, and B.A. Remington, Bull. Am. Phys. Soc., **43**, 1731 (1998), paper F3S38.
40. D. Ryutov *et al.*, submitted, Ap. J. Suppl. (Jan. 1999).
41. R.A. Chevalier, Science **276**, 1374 (1997); T. Suzuki and K. Nomoto, Ap. J. **455**, 658 (1995); C. Fransson *et al.*, *ibid* **461**, 993 (1996); J.M. Marcaide *et al.*, Science **270**, 1475 (1995); R.A. Chevalier and C. Fransson, Ap. J. **420**, 268 (1994).
42. J.C. Bozier, J.P. Le Breton, *et al.*, Phys. Rev. Lett. **57**, 1304 (1986).
43. T. Afshar-rad *et al.*, Phys. Rev. Lett. **73**, 74 (1994).
44. D. Hoarty *et al.*, Phys. Rev. Lett. **78**, 3322 (1997).
45. Tsvi Piran, in *Unsolved Problems in Astrophysics*, by John N. Bahcall and Jeremiah P. Ostriker (Princeton University Press, Princeton, New Jersey, 1997), pp. 343-369.
46. G.J. Fishman & C.A. Megan, in Ann. Rev. Astron. Astrophysics **33**, 415 (1995).
47. E. Waxman, Ap. J. **489**, L33 (1997).
48. E. Waxman, submitted, Ap. J. Suppl. (Jan. 1999).
49. J.H. Krolick & E.A. Pier, Ap. J. **373**, 227 (1991).
50. E. Liang, M. Kusunose, I. A. Smith, A. Crider, Ap.J. **479**, L35-L38 (1997).
51. D. Farley *et al.*, submitted, Phys. Rev. Lett. (March 1999).
52. M.H. Key *et al.*, Phys. Plasmas **5**, 1966 (1998).
53. T. Cowan *et al.*, in Proc. of XXIV ECLIM, to be published in Lasers and Particle Beams (1999); and in preparation for submittal to PRL (1999).
54. W.B. Hubbard *et al.*, Phys. Plasmas 4, 2011 (1997).
55. D. Saumon *et al.*, Phys; Rev. Lett. **76**, 1240 (1996); Ap. J. **460**, 993 (1996).
56. T. Nakajima *et al.*, Nature **378**, 463 (1995); B.R. Oppenheimer *et al.*, Science **270**, 1478 (1995).
57. G. W. Collins *et al.*, Science **281**, 1178 (1998); Phys. Plasmas **5**, 1864 (1998); L. B. Da-Silva *et al.*, Phys. Rev. Lett. **78**, 483-6 (1997).
58. S.T. Weir, A.C. Mitchell, and W.J. Nellis, Phys. Rev. Lett. **76**, 1860 (1996).
59. N.C. Holmes, M. Ross, and W.J. Nellis, Phys. Rev. B 52, 15835 (1995).
60. W.J. Nellis, submitted, J. Planetary and Space Sciences (Sept. 1998).
61. W. J. Nellis, M. Ross, N. C. Holmes, Science **269**, 1249-52 (1995).
62. M. Koenig *et al.*, submitted, Ap. J. Suppl. (Jan. 1999); Phys. Rev. Lett. **74**, 2260 (1995).
63. A. Benuzzi *et al.*, Phys. Rev. E 54, 2162 (1996).
64. A.M. Evans *et al.*, Laser and Part. Beams **14**, 113 (1996).
65. T. Lower *et al.*, Phys. Rev. Lett. **80**, 4000 (1998); M. Basko *et al.*, Phys. Rev. E **56**, 1019 (1997); T.A. Hall *et al.*, Phys. Rev. E **55**, R6356 (1997).
66. T. Lower *et al.*, Phys. Rev. Lett. **72**, 3186 (1994).
67. S. Fu *et al.*, Phys. Plasmas **2**, 3461 (1995).

## FIGURE CAPTIONS

Fig. 1. Supernova light curves and opacities. (a) Calculated light curves for SN1987A (reproduced from ref. 4). (b) Modeling and experimental measurements of the opacity of Fe at a temperature of T = 20 eV (reproduced from ref. 13). (c) Experimental measurements of radiation line transport through an expanding Al plasma with a large velocity gradient (reproduced from ref. 14).

Fig. 2. Mixing in supernova explosion hydrodynamics. (a) Image of simulated hydrodynamic mixing from SN1987A at t = 12000 s (reproduced from ref. 15). (b) An image from a laser experiment designed to measure this hydrodynamic mixing of a $\lambda$=200 $\mu$m wavelength ripple under scaled conditions at t=35 ns (reproduced from ref. 17).

Fig. 3. Young supernova remnant dynamics. (a) Observational image of the inner circumstellar ring of SN1987A (http://antwrp.gsfc.nasa.gov/apod/ap980217.html). (b) Image from shock experiments designed to produce similar, scaled regimes of strong shock hydrodynamics (reproduced from ref. 30).

Fig. 4. Shocks in older supernova remnants. (a) Observational image of SN1006 (http://www-cr.scphys.kyoto-u.ac.jp/research/pix/sn1006_i.gif). (b) Spectral analysis of the shocks from SN1006 (reproduced from ref. 24). (c) Experimental image of a shock launched by a 40 fs, 15 mJ laser pulse in a gas cluster target, and diagnosed by optical interometry (ref. 39). (d) Spectral analysis of experimentally generated shocks in foam targets, from which the temperature behind shock front can be determined (reproduced from refs. 43, 44).

Fig. 5. Gamma ray bursts and relativistic plasmas. (a) Time evolution of the photon burst detected from GRB920110 (repoduced from ref. 46). (b) Experimental $\gamma$-ray energy spectrum from GRB910601 (reproduced from ref. 46). (c) Calculation of a GRB spectrum (reproduced from ref. 50). (d) Measured electron energy spectrum from Petawatt laser experiments (reproduced from ref. 53). (e) Measured x-ray energy spectrum from experiments using the Petawatt laser (reproduced from ref. 52).

Fig. 6. The phase diagram and equation-of-state (EOS) experiments relevant to the giant planets and brown dwarfs. (a) Theoretical phase diagram of hydrogen (reproduced from ref. 57) relevant to Jupiter and the brown dwarf G1229B. (b) Measured compression (density) versus shock-induced pressure, that is, the measured principle Hugoniot for cryogenic liquid $D_2$ (reproduced from ref. 57).

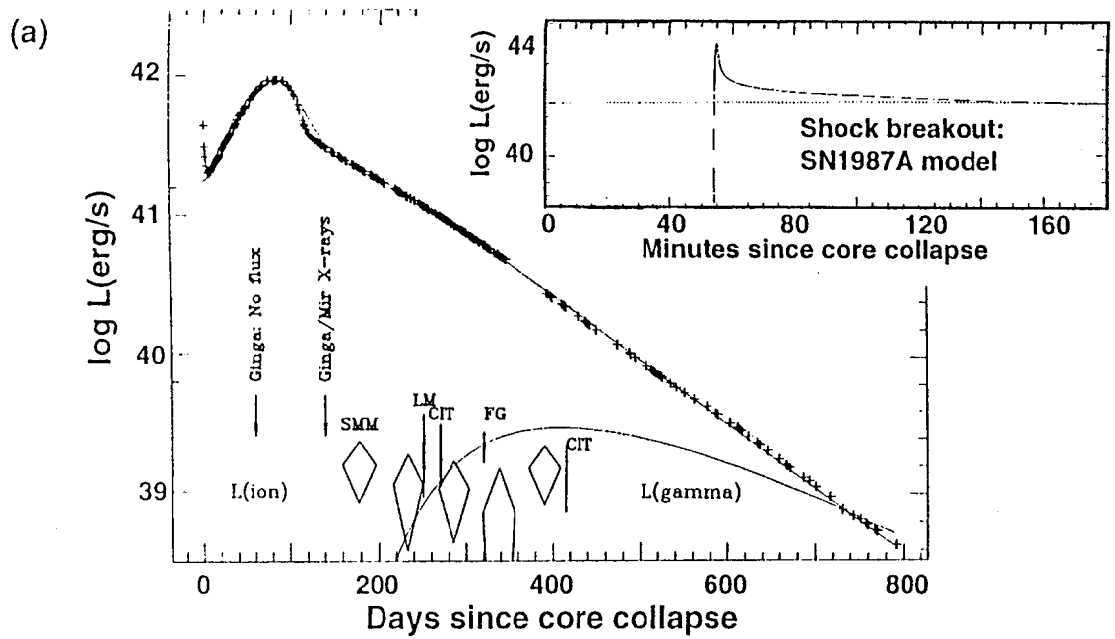


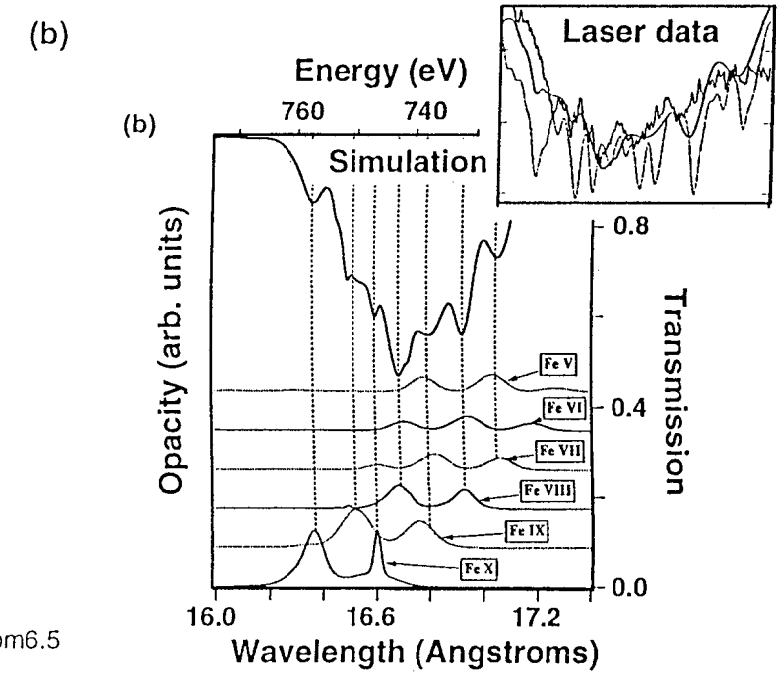


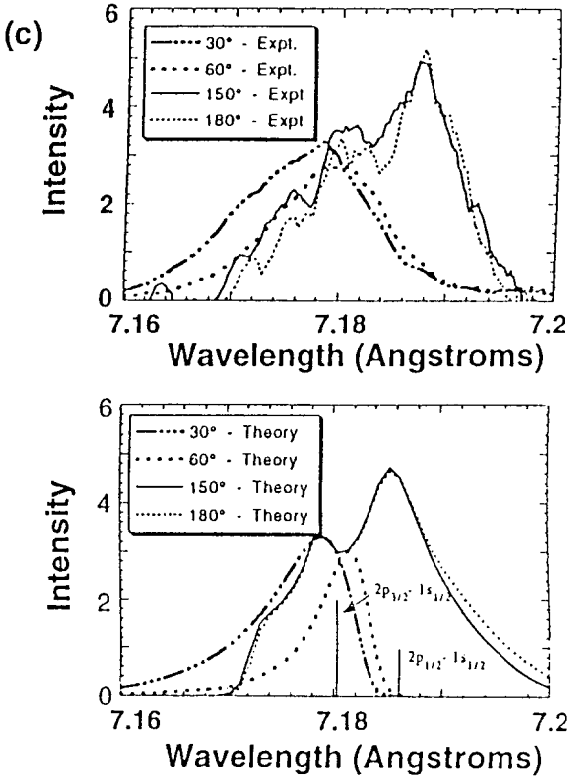


Figure_1/Science.pm6.5

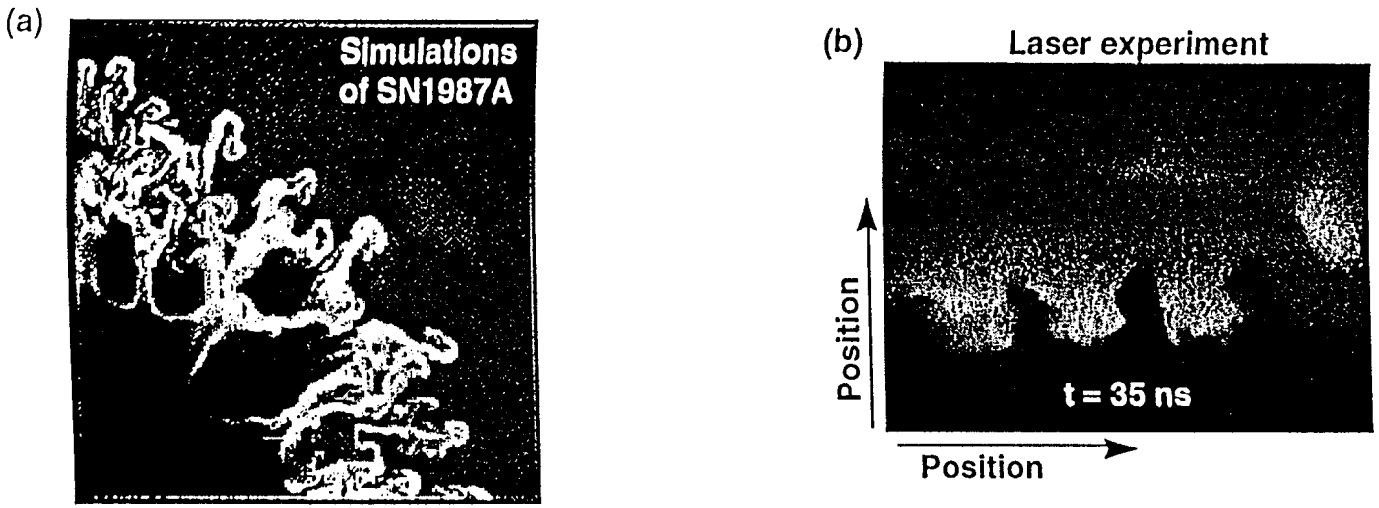


Figure 2

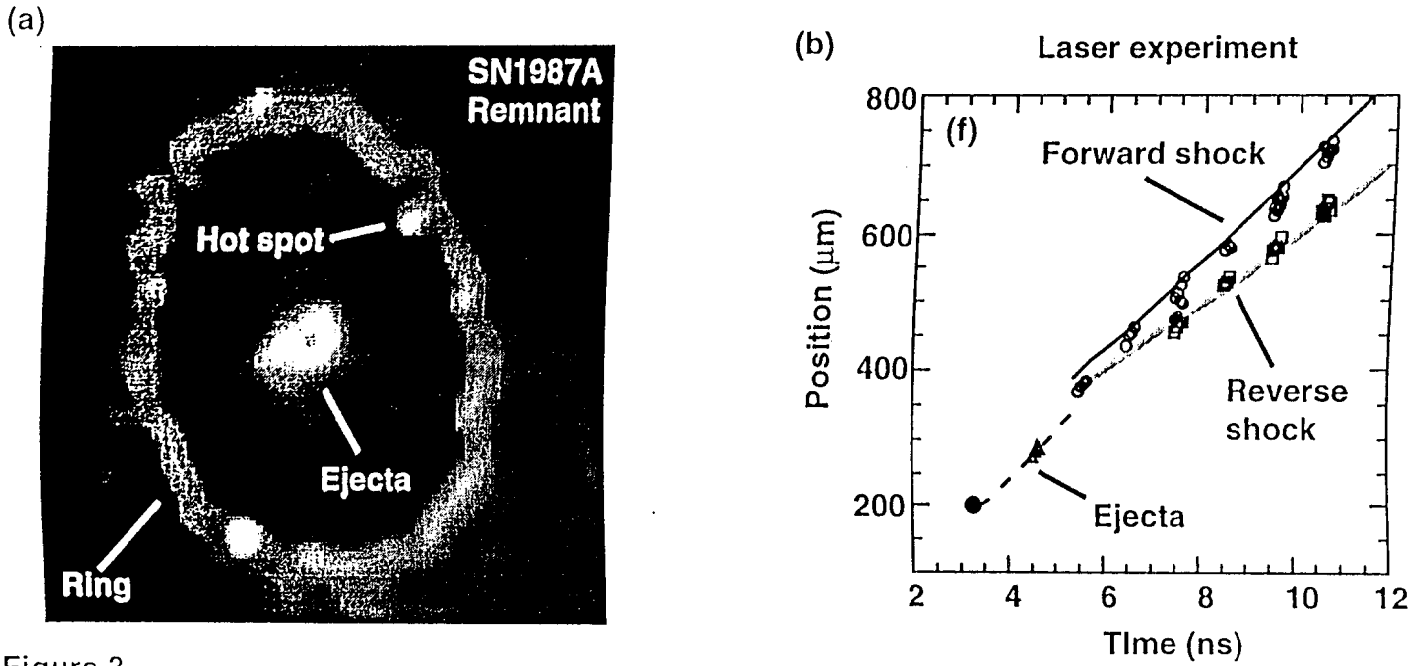


Figure 3

Figure_2,3/Science.pm6.5

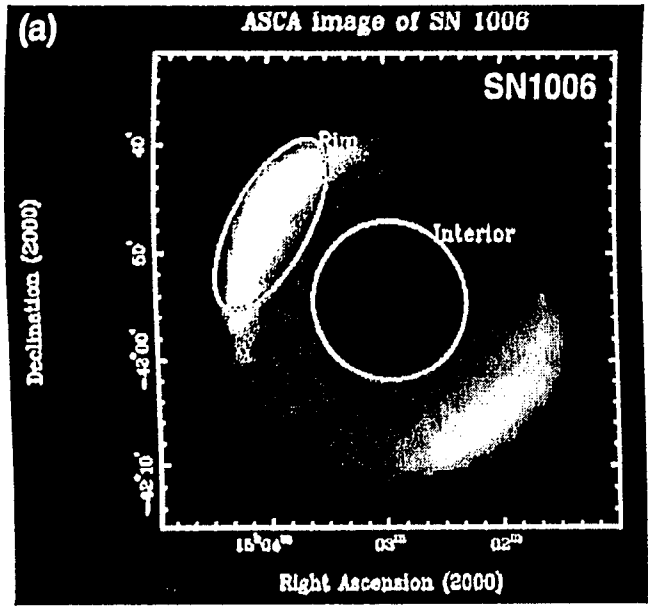


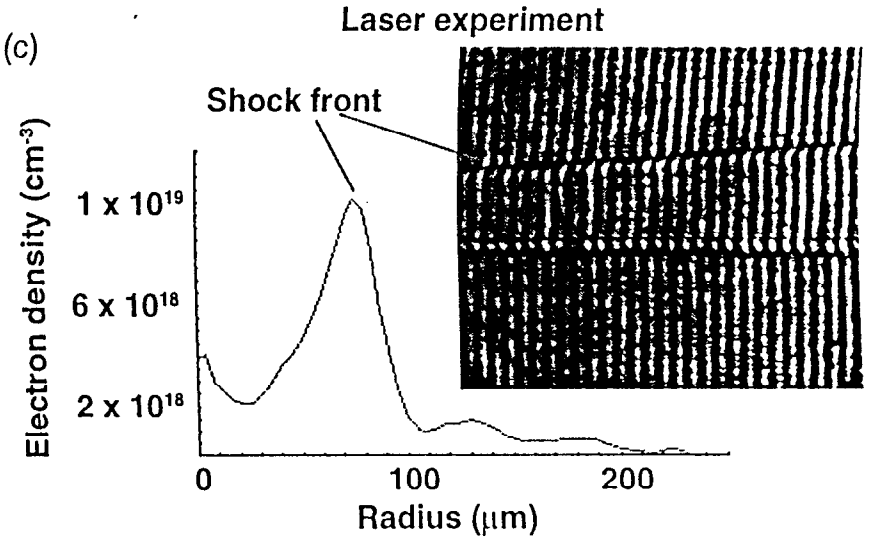


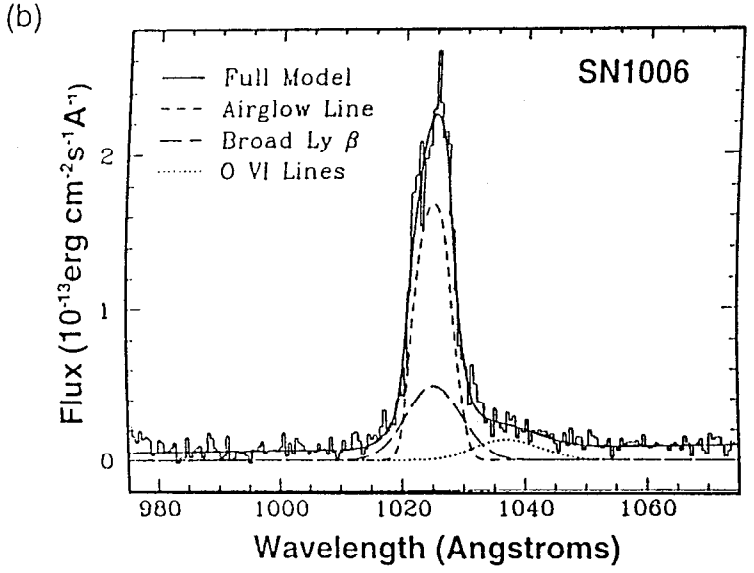


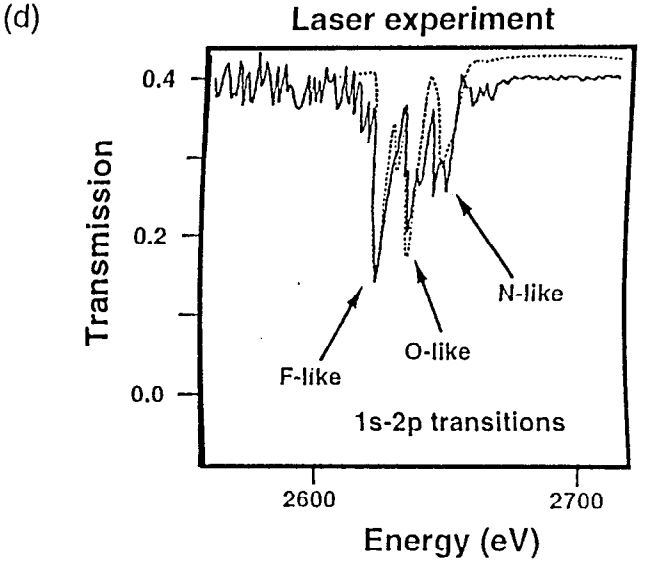


Figure_4/Science.pm6.5

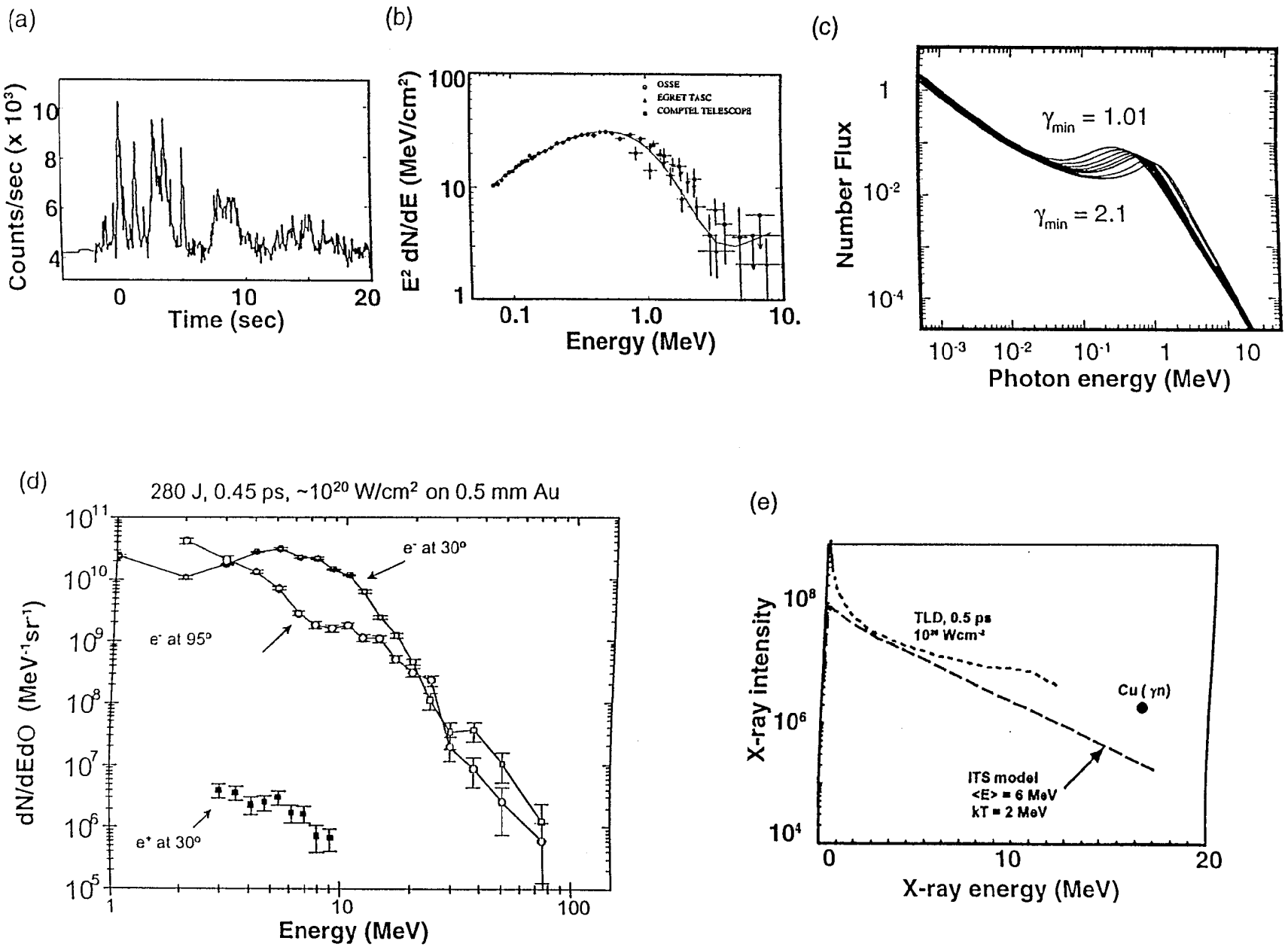


Figure_5/Science.pm6.5

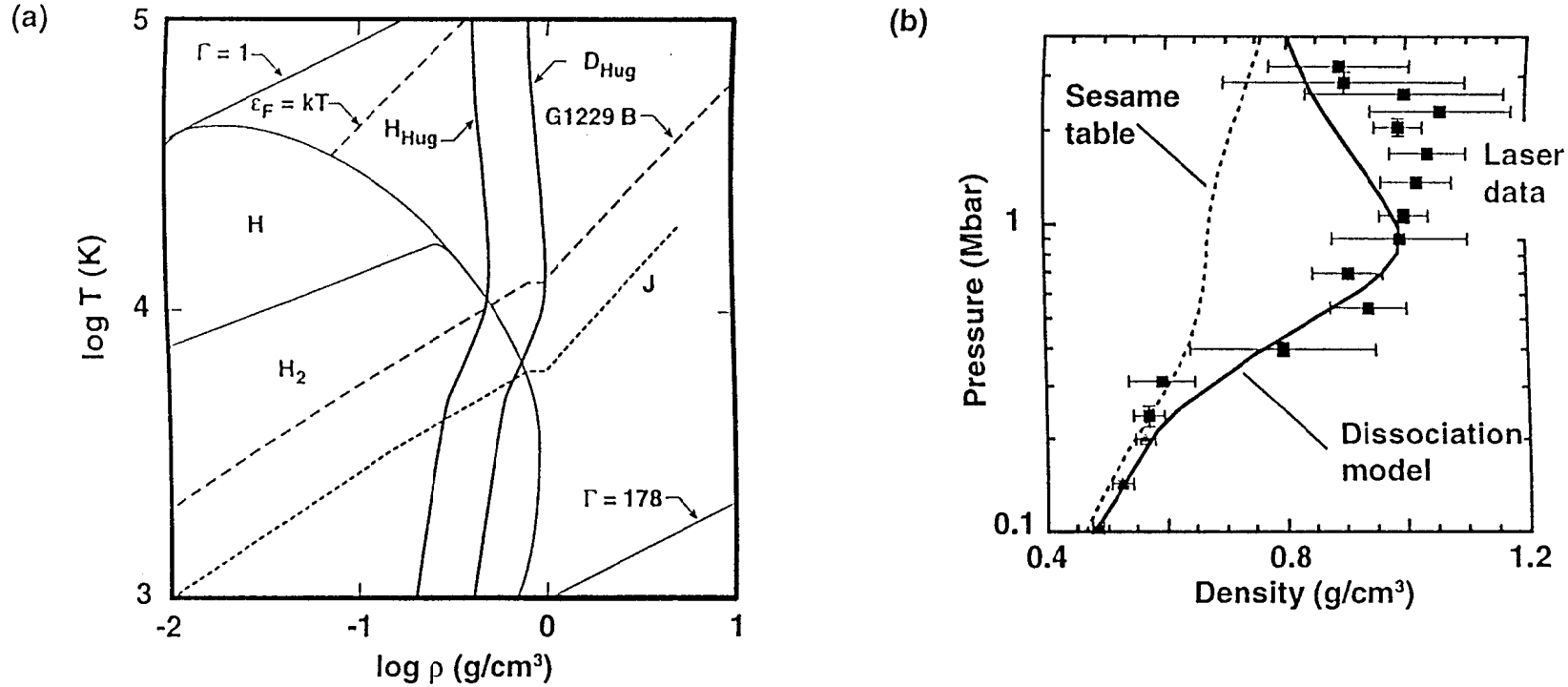


Figure_6/Science.pm6.5